Resonant propulsion of a microparticle by a surface wave

A. V. Maslov*
University of Nizhny Novgorod, Nizhny Novgorod, 603950, Russia

V. N. Astratov
Department of Physics and Optical Science, Center for Optoelectronics and Optical Communication, University of North Carolina at Charlotte, Charlotte, North Carolina 28223-0001, USA

M. I. Bakunov
University of Nizhny Novgorod, Nizhny Novgorod, 603950, Russia
(Received 5 March 2013; published 30 May 2013)

We investigate the electromagnetic force experienced by a microparticle supporting high-quality whispering gallery modes that are excited by a surface wave. Our theoretical approach is based on an analytical representation of the solution of the scattering problem with a subsequent numerical treatment. It accounts rigorously for the interaction of the microparticle with the waveguiding surface and allows us to establish the balances of electromagnetic power and momentum flow for the system. We show that the resonant excitation of the whispering gallery modes and suppression of the transmitted surface wave lead to an almost complete transformation of the momentum flow of the initial surface wave into the propelling force on the microparticle. The validation of the momentum balance justifies the definition of the momentum flow of the surface wave as the ratio of carried power and phase velocity. A simple approximate relation between the propelling force and the power of the transmitted surface wave is also introduced. The transverse force can be either attractive or repulsive depending on the particle-to-surface distance, particle size, and operating frequencies, and it can significantly exceed the value of the propelling force. A comparison with a microparticle excited by a plane wave is also included.

DOI: 10.1103/PhysRevA.87.053848 PACS number(s): 42.50.Wk, 42.60.Da, 42.25.Fx

I. INTRODUCTION

The incidence of a focused electromagnetic beam on a microparticle can lead to its significant acceleration due to the smallness of the particle mass. This was the original motivation behind the optical trapping and manipulation of neutral microparticles using lasers [1]. The magnitude of the electromagnetic force is determined by the amount of radiation absorbed or scattered by the microparticle. In typical experimental cases with dielectric microparticles, especially immersed in liquids, the smallness of the refractive index contrast gives rise to forces that are significantly smaller as compared to the case of total absorption. The low efficiency of power-to-force transformation may be counteracted by increasing the power of the electromagnetic beam, but this is not always possible or desirable.

One of the ways to increase the electromagnetic force is to use some resonant properties of microparticles. Resonances, for example, can exist in small metal particles. Another interesting direction is to use dielectric microparticles with relatively large sizes that support high-quality (Q) whispering gallery modes (WGMs). Although the appearance of peaks of the optical force due to the excitation of WGMs was experimentally demonstrated in Ref. [2], no significant enhancement of force was observed. It was proposed that the experiments [2] detected only third- or higher-order WGMs with lower Q factors, while first- and second-order modes with the highest Q factors were not detected, either due to insufficient instrumental resolution or the presence of weak absorption or irregularities of shape [3]. The reason for only a weak enhancement of the optical forces was the low efficiency of light coupling from a laser beam to the WGMs of the microparticles. The most common way to increase the coupling is to use waveguiding modes or prisms that create evanescent tails due to total internal reflection [4]. These schemes form the foundations of multiple applications of WGMs that appeared recently [5].

The emergence of new applications of WGM resonances stimulated renewed attention (both theoretical and experimental) to the optical forces that result from the excitation of WGMs. The interest lies in the development of optofluidic technologies aimed at manipulating microparticles and sorting them according to the positions of their WGM peaks. These technologies may result in creating integrated microsphere resonator circuits [6]. From the theoretical side, earlier works studied the force on particles using a plane-wave excitation based on the Mie theory and predicted weak force oscillations as a function of the size parameter [7]. Using an infinitely extended evanescent tail (to model the behavior of a guided mode with a reduced phase velocity) gives much larger oscillations of force due to a more efficient excitation of WGMs [8]. However, the infinitely extended evanescent tail does not allow one to evaluate the efficiency of the excitation since the available power is not limited. A similar model was used for the prism excitation [9]. The force in the prism-coupling geometry was also studied numerically considering the interaction of the surface and the resonator in two-dimensional (2D) geometry [10]. Although this configuration allows one to obtain significant excitation of WGMs

*avmaslov@yandex.ru

and a large peak-to-background ratio in the force spectra, the evaluation of the excitation efficiency was complicated by the fact that the incident plane wave had infinite power. Monotonic growth of force with diameter (without WGM-based enhancement) was also calculated recently for particles smaller than 0.9 μm excited by a fiber mode [11].

From the experimental side, the measurement of the propelling force on microparticles with diameters 3–12 μm created by the evanescent tail of a waveguiding mode showed no oscillations but only an increase with their diameter [12]. The lack of oscillations was attributed to the deviations in the particle diameters. The velocity of particles showed a linear dependence on the diameter (that translates into a quadratic dependence of force) for sizes 0.5–3 μm [13].

From a more general point of view, there is a significant amount of interest in studying the nanoscale optomechanical properties of integrated photonic circuits. This includes the investigation of forces between chip-scale waveguides [14,15], the enhancement of force on a waveguide evanescently coupled to a high-Q microdisk resonator [16], and the enhancement of force acting on particles in the vicinity of photonic crystal cavities [17,18] or inside resonators [19].

The appearance of large and highly size-selective propelling forces on liquid-immersed microparticles with diameters 10–20 μm has been demonstrated very recently [20,21]. The experiments were performed with simultaneous control of the WGM resonances in the fiber-to-microsphere couplers [22]. Estimates of force based on Stokes' law showed that the measured velocities correspond to a 60% power absorption from the exciting mode of the optical fiber. The magnitude and selectivity of the force were interpreted as a result of WGM excitation based on a theoretical model and supporting simulations. The purpose of this paper is to investigate in detail the force (both the propelling and transverse components) on microparticles due to the excitation of WGMs and evaluate the efficiency of the power-to-force conversion. Some preliminary results for the propelling force were reported in Refs. [20,21] without providing a detailed explanation of the model and of the analytical theory. In this paper, we fill in this gap by describing the model and the theory. We also expand our theoretical treatment by including a comparison with the case of a microparticle in free space and investigating the transverse force. More importantly, we advance the theoretical treatment to include the investigation of the balance of electromagnetic momentum in the system. This allows us to obtain a relation between the electromagnetic momentum and the propelling force, and to explain the large value of the force.

To capture the most relevant physical phenomena related to the excitation of the WGMs of a microparticle by a surface wave, we choose the following physical model of the system. It consists of a cylindrical resonator located near a surface that supports surface waves. This 2D model describes the physical processes of the excitation of the WGMs and interaction of the excited modes with the surface. The evanescent field created by the surface wave has similar properties (decay, phase velocity) to that created by the waveguide modes of a dielectric slab. Finite power and momentum flow carried by the initial wave allow us to investigate their balances in the system during the interaction of the wave and the resonator. Furthermore, since the surface can support only one guided mode and prohibits the wave propagation in the metal, verification of the power and momentum balances is easier than in the case with a dielectric slab. In calculating the forces, we also assume that the cylinder is surrounded by a vacuum rather than liquid. The consistent mathematical model of calculating the forces on dielectric objects in liquids still remains under debate [23]. We therefore address a simplified case in which the cylinder is surrounded by a vacuum, and we focus only on the resonant excitation of its WGMs.

The 2D model allows one to investigate the interaction of the resonator and guided surface very accurately. Although the use of spherical particles would be more desirable, the most commonly used method to study the excitation of WGMs of microspheres relies on neglecting the interaction between the sphere and the waveguide and/or assuming a single mode of the sphere [4]. Such approximations may be difficult to justify since there is no comparison with exact solutions. The commonly used finite-difference time-domain (FDTD) method suffers from various artifacts (for example, the staircase approximation of the surface and numerical dispersion). More importantly, the FDTD method can even completely miss high-Q resonances [24], and that makes it unsuitable for an accurate modeling of high-Q circular resonators both in 2D and 3D geometries. The finite-element method (FEM) is more suitable for treating irregular geometries, but it requires substantial computational resources even in the 2D case [25]. We therefore choose a simpler model that allows a rigorous solution to capture the most relevant physical phenomena over more complicated models that require less justifiable approximations.

The scattering of a surface wave represents a complicated diffraction problem even in 2D geometry. There exist several analytical approaches to tackle it. They are based on using a spectral representation of the polarization current in the resonator [26], using the volume-integral equation based on Green's functions [27], or using effective surface potentials [28,29]. In our case, we expand the fields inside the resonator using the cylindrical functions as bases and represent the fields outside of the resonator using effective magnetic surface currents. Solving the diffraction problem gives the expansion for the fields in terms of the cylindrical functions. The expansion allows one to derive simple formulas for the force by integrating the fields inside the cylinder.

The high numerical accuracy of the computational technique that we use allows us to establish the balance of the power and momentum in the system consisting of the particle and surface. Based on the momentum balance, we can also check the definition of the momentum flow for the surface waves that is appropriate for calculating the force. Such a verification helps to clarify the Abraham-Minkowski controversy [23].

The paper is organized as follows. Section II specifies the physical model, introduces basic equations, and describes the solutions of the scattering problem and calculation of forces. It also introduces the balances of the electromagnetic power and of momentum flow. Results of scattering and force calculation for a plane-wave illumination are presented in Sec. III, and results for surface-wave illumination are presented in Sec. IV. Section V gives our conclusion.

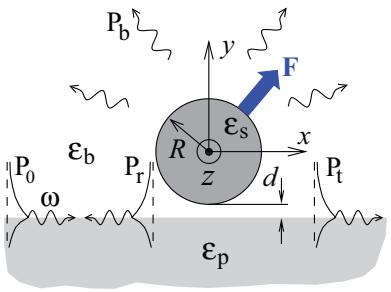

FIG. 1. (Color online) Schematics of scattering of a surface electromagnetic wave guided by the boundary of a metal half-space on a cylinder near the surface.

II. THEORY

A. Physical model

The physical model is specified in Fig. 1. It consists of a dielectric cylinder with the dielectric constant ε_s located in the background medium with the dielectric constant ε_b. The cylinder is brought at a distance d to the interface between the background material and a plasmalike material (metal) with the dielectric constant $\varepsilon_p < 0$ that can support surface waves. An initial surface wave with power P_0 is scattered by the cylinder. The scattering creates a transmitted surface wave with power P_t, a reflected surface wave with power P_r, and bulk waves with power P_b. As a result, the cylinder experiences an electromagnetic force $\mathbf{F}$, which is the subject of our investigation.

B. Outline of the solution

To find the force, we first calculate the electromagnetic fields by solving the scattering problem and then use the fields to obtain the force. The scattering problem is solved by using particular representations for the electromagnetic fields inside and outside of the scattering cylinder and matching the fields using the boundary conditions. To represent the fields, it is convenient to take advantage of the circular symmetry of the scattering cylinder. The fields inside are expanded in terms of the free-space solutions, i.e., cylindrical functions. The fields outside are represented as generated by some effective magnetic currents along the cylindrical surface. The currents can be conveniently expanded in terms of the angular harmonics as well. Matching gives the system of equations to find the expansion coefficients and, therefore, the fields both inside and outside the cylinder. The force is calculated using two alternative methods. One is based on using the Lorentz formula applied to surface polarization charges and bulk currents. The other is based on integrating the Maxwell tensor along a surface outside of the cylinder. The solution of the scattering problem is presented for arbitrary dielectric constants in the system, while the force is calculated only for $\varepsilon_b = 1$.

C. Basic equations and boundary conditions

The initial surface wave that propagates in the $+x$ direction has its magnetic field along the cylinder axis, and no other magnetic components exist. This dictates that only three components of the electromagnetic field $\{E_x, E_y, H_z\}$ are present. We choose to work with complex amplitudes of the field and assume $\sim\exp(-i\omega t)$ time dependence. The frequency ω is set by the initial surface wave. The real fields are assumed to be equal to twice the real part of the corresponding complex counterparts.

We take the Maxwell equations with a z-oriented magnetic current density $J_z^m(\mathbf{r})$, which we will later use as an effective current. Keeping only the nonzero field components, we obtain

$$\frac{\partial E_y}{\partial x} - \frac{\partial E_x}{\partial y} = \frac{i\omega}{c} B_z - \frac{4\pi}{c} J_z^m, \tag{1a}$$

$$\frac{\partial H_z}{\partial y} = -\frac{i\omega}{c} D_x, \tag{1b}$$

$$-\frac{\partial H_z}{\partial x} = -\frac{i\omega}{c} D_y. \tag{1c}$$

In a homogeneous region with the dielectric constant ε, Eqs. (1) can be reduced to an equation for H_z only:

$$\left(\nabla^2 + \frac{\omega^2}{c^2}\varepsilon\right) H_z = -\alpha J_z^m, \tag{2}$$

where ∇ is the nabla operator and $\alpha = 4\pi i\omega\varepsilon/c^2$. Equation (2) is the Helmholtz equation with an excitation proportional to J_z^m. We will use the current density on the cylinder surface only to represent the fields outside of the cylinder. The solutions inside and outside of the cylinder should satisfy the usual boundary conditions—the continuity of the tangential magnetic and electric field components. The electric field can be obtained from the magnetic field using Eqs. (1b) and (1c).

D. Initial surface wave

The magnetic field of the initial surface wave has the following form for $y > -a$:

$$H_z^i(x, y > -a) = B_0 e^{ih_0 x - \varkappa_0 (y+a)}, \tag{3}$$

where H_0 is the value of the magnetic field at the metal boundary and $a = R + d$. The wave number h_0 and the decay constant $\varkappa_0$ are defined by the frequency ω and the constants $\varepsilon_p < 0$ and $\varepsilon_b > 0$ ($|\varepsilon_p| > \varepsilon_b$):

$$h_0 = \frac{\omega}{c}\sqrt{\frac{\varepsilon_p \varepsilon_b}{\varepsilon_p + \varepsilon_b}}, \quad \varkappa_0 = \frac{\omega}{c}\frac{\varepsilon_b}{\sqrt{-\varepsilon_b - \varepsilon_p}} \tag{4}$$

such that $h_0^2 - \varkappa_0^2 = k_b^2$ and $k_b^2 = \omega^2\varepsilon_b/c^2$. The power carried by the surface wave is

$$P_0 = \frac{c^2}{\omega}\frac{|B_0|^2}{4\pi}\frac{h_0}{\varepsilon_b \varkappa_0}\left(1 - \frac{\varepsilon_b^2}{\varepsilon_p^2}\right). \tag{5}$$

We expand the fields of the initial wave (3) at $|\mathbf{r}| = \sqrt{x^2 + y^2} = R$ in terms of the angular harmonics:

$$H_z^i(\mathbf{r}) = \sum_n e^{in\varphi} H_{zn}^i, \quad E_\varphi^i(\mathbf{r}) = \sum_n e^{in\varphi} E_{\varphi n}^i. \tag{6}$$

The sums are for $-\infty < n < \infty$ but are limited in the numerical algorithms. The expansion coefficients in Eq. (6) are

$$H_{zn}^i = H_0 e^{-\varkappa_0 a} i^n \left(\frac{h_0 + \varkappa_0}{k_b}\right)^n J_n(k_b R), \tag{7a}$$

$$E_{\varphi n}^i = H_0 e^{-\varkappa_0 a} \frac{-ick_b}{\omega\varepsilon_b} i^n \left(\frac{h_0 + \varkappa_0}{k_b}\right)^n J_n'(k_b R), \tag{7b}$$

where $J_n(\xi)$ is the Bessel function of the first kind of order n and $J_n'(\xi)$ is its derivative.

E. Representation of the solution

We represent the total field inside the cylinder in terms of the cylindrical functions:

$$H_z(\mathbf{r}) = \sum_n A_n J_n(k_s r) e^{in\varphi}, \quad r < R, \tag{8}$$

$$E_\varphi(\mathbf{r}) = \frac{-ick_s}{\omega\varepsilon_s} \sum_n A_n J_n'(k_s r) e^{in\varphi}, \quad r < R, \tag{9}$$

where A_n are some unknown complex coefficients.

The total field outside of the cylinder can be represented as a sum of the initial field (3) and scattered field:

$$H_z(\mathbf{r}) = H_z^s(\mathbf{r}) + H_z^i(\mathbf{r}). \tag{10}$$

The scattered field can be represented as a field created by some effective magnetic current $j(\varphi)$ localized on the cylinder surface:

$$H_z^s(\mathbf{r}) = \int_0^{2\pi} d\varphi'\ j(\varphi') G(\mathbf{r},\mathbf{r}'). \tag{11}$$

The Green's function $G(\mathbf{r},\mathbf{r}')$ is for the system consisting of the background material and metal. Its calculation is presented in Sec. II F. In principle, we can also use electric currents on the surface [30].

We define the following expansion of an arbitrary function $f(\varphi)$ into the angular harmonics:

$$f(\varphi) = \sum_{n=-\infty}^{\infty} f_n e^{in\varphi}, \quad f_n = \frac{1}{2\pi}\int_0^{2\pi} d\varphi\ f(\varphi) e^{-in\varphi}. \tag{12}$$

Just outside of the cylinder, we obtain the angular components of the fields:

$$H_{zm}^s = \sum_n G_{mn} j_n, \tag{13}$$

$$E_{\varphi m}^s = \frac{-ic}{\omega\varepsilon_b}\left(-\frac{j_m}{2R} + \sum_n \partial_r G_{mn} j_n\right), \tag{14}$$

where the expansion coefficients for the Green's function are defined using

$$G_{mn} = \frac{1}{2\pi}\int_0^{2\pi} d\varphi \int_0^{2\pi} d\varphi'\ G(r,r') e^{-im\varphi + in\varphi'}, \tag{15a}$$

$$\partial_r G_{mn} = \frac{1}{2\pi}\int_0^{2\pi} d\varphi \int_0^{2\pi} d\varphi'\ \partial_r G(r,r') e^{-im\varphi + in\varphi'}. \tag{15b}$$

Note that G is a singular function and its derivative must be handled properly [31].

F. The Green's function for the two half-spaces

To find the Green's function G that enters (11), we take

$$J_z^m(\mathbf{r}) = \frac{1}{\alpha_b}\delta(x-x')\delta(y-y') \tag{16}$$

and solve (1). The solution for H_z is $G(\mathbf{r},\mathbf{r}')$. The solution is obtained by expanding (16) into the Fourier integral representing the current density as a superposition of current sheets with the x dependence as $\sim e^{ihx}$. This reduces the problem to finding the fields in all regions: in the background material (above and below the current sheet) and in the metal. Writing down the solution in all regions as plane waves with fixed h and matching the fields by the boundary conditions and then taking the inverse Fourier integrals gives the solution [32]. We can then represent the Green's function for the two half-spaces as two terms:

$$G(\mathbf{r};\mathbf{r}') = G^0(\mathbf{r};\mathbf{r}') + G^1(\mathbf{r};\mathbf{r}'). \tag{17}$$

The first term is the Green's function for the homogeneous background medium with ε_b. The second term is the remaining contribution due to the presence of the metal. They have the following form:

$$G^0(\mathbf{r};\mathbf{r}') = \frac{i}{4\pi}\int_{-\infty}^{\infty} dh\ \frac{e^{ih(x-x')}}{g_b(h)} e^{ig_b|y-y'|}, \tag{18a}$$

$$G^1(\mathbf{r};\mathbf{r}') = \frac{i}{4\pi}\int_{-\infty}^{\infty} dh\ \frac{e^{ih(x-x')}}{g_b(h)} r_{bp}(h) e^{ig_b(y+y'+2a)}. \tag{18b}$$

The reflection coefficient $r_{bp}(h)$ in Eq. (18b) is for an obliquely incident plane wave from the metal boundary:

$$r_{bp}(h) = \frac{g_b(h)/\varepsilon_b - g_p(h)/\varepsilon_p}{g_b(h)/\varepsilon_b + g_p(h)/\varepsilon_p}, \tag{19}$$

where $g_b(h) = \sqrt{\omega^2\varepsilon_b/c^2 - h^2}$ and $g_p(h) = \sqrt{\omega^2\varepsilon_p/c^2 - h^2}$ describe the y components of the waves in the background material and in the metal, respectively.

For $G^0(\mathbf{r};\mathbf{r}')$ we can evaluate the integral in Eq. (18a) analytically and obtain

$$G^0(\mathbf{r};\mathbf{r}') = \frac{i}{4} H_0(k_b|\mathbf{r}-\mathbf{r}'|), \tag{20}$$

where H_0 is the Hankel function of the first kind.

The coefficients defined by (15) become

$$G_{mn}^0 = \delta_{mn} i\frac{\pi}{2} J_n(k_b R) H_n(k_b R), \tag{21a}$$

$$\partial_r G_{mn}^0 = \delta_{mn}\left(\frac{1}{2R} + i\frac{\pi}{2} k_b J_n(k_b R) H_n'(k_b R)\right), \tag{21b}$$

and

$$G_{mn}^1 = \frac{i}{2} i^{m-n} J_m(k_b R) J_n(k_b R) f_{m+n}, \tag{22a}$$

$$\partial_r G_{mn}^1 = \frac{i}{2} i^{m-n} k_b J_m'(k_b R) J_n(k_b R) f_{m+n}, \tag{22b}$$

where

$$f_n = \int_{-\infty}^{\infty} dh\ \frac{r_{bp}(h)}{g_b(h)} e^{2ig_b(h)a}\left(\frac{h - ig_b(h)}{k_b}\right)^n. \tag{23}$$

Integral (23) has two singularities related to the excitation of the forward and backward surface waves. It also has two branches corresponding to the double-valued function $g_b(h)$.

G. Equation for the expansion coefficients

Matching the expansions of H_z and E_φ gives the following set of equations for finding the expansion coefficients A_m

and j_m:

$$A_m J_m(k_s R) - \sum_n G_{mn} j_n = H^i_{zm}, \quad (24a)$$

$$\frac{k_s}{\varepsilon_s} A_m J'_m(k_s R) + \frac{1}{\varepsilon_b}\left[\frac{j_m}{2R} - \sum_n \partial_r G_{mn} j_n\right] = \frac{i\omega}{c} E^i_{\varphi m}. \quad (24b)$$

We can eliminate A_n from these equations, and by applying expansions (7), (21), and (22) we obtain a set of equations for finding j_m:

$$\sum_n M_{mn} j_n = F_m, \quad (25)$$

where

$$M_{mn} = \delta_{mn} + \frac{i^m}{\pi J_m(k_b R)(1 + i\Delta_m)} i^{-n} J_n(k_b R) f_{m+n},$$

$$F_m = \frac{i^m}{\pi J_m(k_b R)(1 + i\Delta_m)} 2i B_0 e^{-\varkappa_0 a}\left(\frac{h_0 + \varkappa_0}{k_b}\right)^m,$$

$$\Delta_m = \frac{(k_s/\varepsilon_s) Y_m(b) J'_m(s) - (k_b/\varepsilon_b) Y'_m(b) J_m(s)}{(k_s/\varepsilon_s) J_m(b) J'_m(s) - (k_b/\varepsilon_b) J'_m(b) J_m(s)},$$

$b = k_b R$, and $s = k_s R$. Similar equations can be obtained by using the approach based on effective surface potentials that create the fields inside and outside of the cylinder [29] and by using the spectral decomposition of the polarization current [26]. Solving (25) numerically gives the current density from which all fields can be calculated.

H. Electromagnetic force

The most direct way to calculate the electromagnetic force is to use the formula for the distributed Lorentz force acting on the dielectric object:

$$\mathbf{F} = \int d\ell\, \sigma \mathbf{E}_\sigma + \frac{1}{c}\iint dS \frac{\partial \mathbf{P}}{\partial t} \times \mathbf{B}. \quad (26)$$

The first term in Eq. (26) describes the sum of all forces acting on small surface polarization charges $\sigma d\ell$ due to the presence of the field $\mathbf{E}_\sigma$ created by other sources. The second term describes the force acting on the bulk polarization current. The electric component of the force appears only on the surface of the cylinder due to polarization charges, while the magnetic component is distributed over the volume.

Using the representation of the fields (8) and integrating (26), we obtain for the x component of the force

$$F_x = F^e_x + F^m_x, \quad (27)$$

where the electric F^e_x and magnetic F^m_x contributions are

$$F^e_x = \frac{(\varepsilon_s - 1)}{2\varepsilon_s^{3/2}} \frac{c}{\omega} \sum_n \mathrm{Re}(A_n A^*_{n+1})\Big[(n+1) J^2_{n+1}(s) + n J^2_n(s) + (\varepsilon_s - 1)\frac{1}{s} n(n+1) J_n(s) J_{n+1}(s)\Big], \quad (28)$$

$$F^m_x = -\frac{\varepsilon_s - 1}{2\varepsilon_s^{3/2}} \frac{c}{\omega} s \sum_n \mathrm{Re}(A_n A^*_{n+1}) J_n(s) J_{n+1}(s), \quad (29)$$

$s = k_s R = R\sqrt{\varepsilon_s}\omega/c$, and $\mathrm{Re}(\xi)$ denotes the real part of a complex number ξ. The y components of the force can be calculated by taking the imaginary part instead of the real part in Eqs. (28) and (29). Expressions (28) and (29) allow one to calculate the forces without any time-consuming integration procedures since all integrations were carried out analytically using the cylindrical functions. The force can also be calculated using the Maxwell tensor integrated over the surface of the cylinder. We implemented both approaches and obtained identical results.

I. The balance of electromagnetic power and momentum flow

The scattering of the initial surface waves results in the creation of the transmitted surface wave, the reflected surface wave, and bulk radiation in the background material. Calculating the powers of these waves allows one to check the power balance to verify the analytical derivation and numerical implementation.

The amplitudes of the scattered surface waves are found as residues of integral (11). The residues occur at the points $h = \pm h_0$ and correspond to the excitation of the forward and backward surface waves. Their amplitudes at $y = -a$ are

$$H^\pm_z = \frac{i\pi}{\varkappa_0} e^{-\varkappa_0 a} \operatorname*{Res}_{h=h_0}(r_{bp}) \times \sum_n j_n (-i)^n \left(\frac{\varkappa_0 \pm h_0}{k_b}\right)^n J_n(k_b R), \quad (30)$$

where Res denotes the residue. The amplitude of the forward wave H^+_z must be added to the initial wave to determine the amplitude of the transmitted wave. The powers of the transmitted P_t and reflected P_r surface waves are determined in same manner as for the initial wave using Eq. (5).

The waves in the background material far away from the cylinder have a typical far-field form at $r \to \infty$. It can be obtained using the asymptotic representation of the Hankel function and Eq. (11):

$$H_z(\mathbf{r}) \approx \frac{f(\varphi)}{\sqrt{k_b r}} e^{-i\pi/4 + ik_b r}, \quad (31)$$

where the far-field distribution $f(\varphi)$ $(0 < \varphi < \pi)$ is

$$f(\varphi) = i\sqrt{\frac{\pi}{2}} \sum_n j_n (-i)^n J_n(k_b R) \times [e^{in\varphi} + r_{bp}(k_b \cos\varphi) e^{-in\varphi + 2ik_b a \sin\varphi}]. \quad (32)$$

The power of the bulk radiation P_b becomes

$$P_b = \int_0^\pi d\varphi\; S_b(\varphi), \quad S_b(\varphi) = \frac{c^2}{\omega} \frac{1}{2\pi\varepsilon_b} |f(\varphi)|^2, \quad (33)$$

where $S_b(\varphi)$ is the bulk power scattered in the background material per unit angle.

The required power balance reads

$$P_0 = P_t + P_r + P_b. \quad (34)$$

The momentum flow M_0 of the initial surface wave in the $+x$ direction is related to its power P_0 by

$$M_0 = \frac{P_0}{v_{\mathrm{ph}}} = \frac{n_{\mathrm{ph}} P_0}{c}, \quad (35)$$

where v_{ph} is the phase velocity and n_{ph} is the phase index [33,34]. Similar expressions are valid for the momentum flow of the transmitted M_t and reflected M_r surface waves. However, we must note that the exact expression for the momentum

flux in a material is still debated [23]. The verification of the momentum balance can potentially clarify whether the expression (35) is consistent with the force calculation.

We can also calculate the momentum flow of the bulk waves in the x and y directions (for $\varepsilon_b = 1$):

$$M_{bx} = \frac{1}{c}\int_0^{\pi} d\varphi S_b(\varphi)\cos\varphi, \quad M_{by} = \frac{1}{c}\int_0^{\pi} d\varphi S_b(\varphi)\sin\varphi. \tag{36}$$

The balance of the momentum flow for the x direction gives

$$\Delta M = M_0 - (M_t - M_r + M_{bx}) = F_x. \tag{37}$$

The difference ΔM corresponds to the x component of force experienced by the system consisting of the cylinder and the half-space region. We will show later that the force on the half-space is zero and the force in Eq. (37) must be attributed to that on the cylinder only. This force should coincide with that calculated using Eqs. (28) and (29).

III. SCATTERING AND FORCE CREATED BY A PLANE WAVE

We first consider the case in which the cylinder is located in free space and illuminated by a plane wave. This allows us to identify various modes of the cylinder, the efficiency of their excitation, and the resultant propelling force. The scattering of a plane electromagnetic wave by a cylinder is a classical problem, but its analysis requires a numerical implementation. The solution also follows from the more general approach that we presented in Sec. II. The knowledge of the fields allows one to find the total scattering cross section and the force. The force can be calculated using Eq. (28). It is convenient to introduce the dimensionless size parameter kR where $k = \omega/c$ and analyze the results depending on its values.

In our analysis, we choose $\varepsilon_b = 1$ and $n_s = \sqrt{\varepsilon_s} = 1.2, 1.4$. The dependence of the scattering cross section and force on kR in a large interval ($0 < kR < 40$) is shown in Fig. 2 and on a small interval ($30 < kR < 32$) in Fig. 3. To normalize the force, we take the power P_0 incident on the cylinder, i.e., area of size $2R$. The quantity cF_x/P_0 can also be referred to as the normalized cross section for radiation pressure [7].

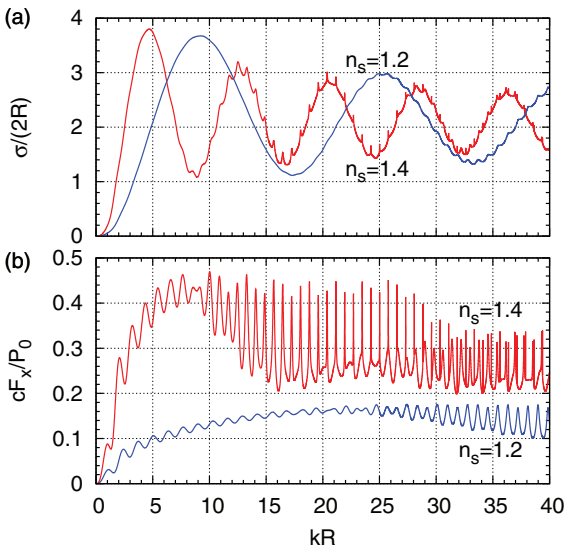

FIG. 2. (Color online) (a) The scattering cross section $\sigma/(2R)$ for a cylinder and (b) the propulsion force cF_x/P_0 as functions of kR for $n_s = 1.2, 1.4$.

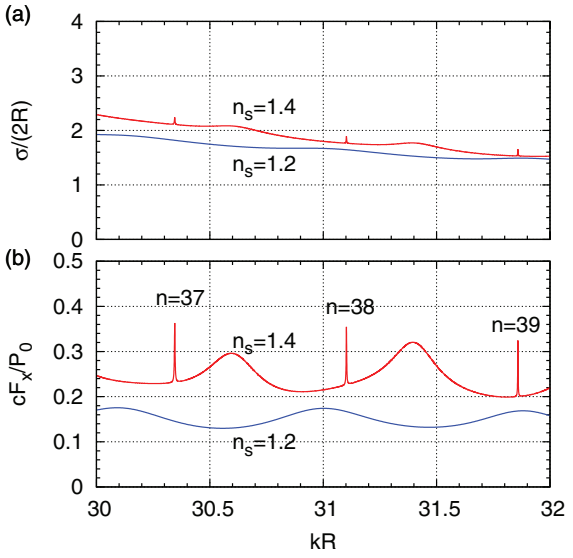

FIG. 3. (Color online) Same as Fig. 2 but focused on a smaller interval of kR. The resonances labeled by their azimuthal numbers $n = 37, 38, 39$ correspond to the first-order WGMs.

For a small kR, the scattering cross section is

$$\frac{\sigma}{2R} \approx \left(\frac{\pi}{2}\right)^2 \left(\frac{\varepsilon_s - \varepsilon_b}{\varepsilon_s + \varepsilon_b}\right)^2 \varepsilon_b^{3/2} (kR)^3, \tag{38}$$

while for $kR \to \infty$ we obtain $\sigma/(2R) \to 2$. An analysis of data from Fig. 2 also gives a $\sim(kR)^3$ behavior for the force at $kR \ll 1$.

The large-scale oscillations of $\sigma(kR)$ correspond to the interference between the scattered and directly transmitted waves. These large-scale oscillations are not present for F_x. However, for $kR \lesssim 10$, the force shows some oscillations that are not present in $\sigma(kR)$. The sharp quasiperiodic peaks (minor oscillations) that appear for large values of kR, both for $\sigma(kR)$ and $F_x(kR)$, correspond to the excitation of WGMs. The WGMs in a cylinder are characterized by their radial and azimuthal numbers. We will focus only on the WGMs that have one maximum in the radial direction inside the cylinder. The number of periods in the azimuthal direction is defined by the azimuthal number n. The range $0 < kR < 40$ covers WGMs of the first order with azimuthal numbers of up to $n = 49$ for $n_s = 1.4$. The WGM peaks for the force are more pronounced than that for the scattering. This is consistent with qualitatively similar results obtained for spheres in free space [7]. However, even for the force, the resonances provide an enhancement of the peak force over its background value by about a factor of 2 or less.

For the lower index $n_s = 1.2$ there is only one minor oscillation, while the higher index case $n_s = 1.4$ shows several higher-order components (with higher WGM radial numbers). For $n_s = 1.4$ and $kR \gtrsim 30$, the fast oscillations tend to merge and become difficult to resolve. However, we verified that our resolution is sufficient so as not to miss any peaks in the studied range of $0 < kR < 40$. The maximum values for the force in

the case of $n_s = 1.4$ become smaller for $kR \gtrsim 30$, but the peaks become denser. It is important to note that although in both cases $n_s = 1.2$ and 1.4 the scattering oscillates around $\sigma/(2R) = 2$, the force shows a tendency to decrease with decrease of n_s.

IV. SCATTERING AND FORCE CREATED BY A SURFACE WAVE

To specify the initial surface wave, we take $\varepsilon_p = -2$, which gives $\varkappa_0 c/\omega = 1$. Therefore, the characteristic decay distance for such a wave in the background region is $1/\varkappa_0 = \lambda/(2\pi)$, where $\lambda = 2\pi c/\omega$. We also take $n_s = 1.4$. Figure 4 shows the results for the powers of the surface and bulk waves as well as created forces on the cylinder for $kd = 1.5$. We note that solving the problem at each frequency takes a fraction of a second with a minimum memory requirement. This compares quite favorably with a similar 2D approach based on a commercial FEM which requires a few minutes for each frequency point with an error of 5% related to discretization [25].

Let us discuss the power dependencies first. In general, we see that the powers are distributed mainly between the transmitted surface wave and bulk radiation. Only a very small fraction of power is going into the reflected surface wave. The power dependence for bulk waves on kR is characterized by a set of peaks with uniform spacing. This contrasts the scattering of a plane wave where the spacing was irregular due to the excitation of various order modes. For small kR, scattering is small and most of the radiation is transmitted unaltered. Increasing kR results in more and more power removed from the transmitted surface wave and converted into the bulk waves. The excitation of the resonant modes of the cylinder facilitates the transfer of power. The transmitted wave can be almost completely suppressed at resonances for $kR \gtrsim 30$.

For the entire range $0 < kR < 40$, the numerical error in the power balance satisfies $|P_t + P_r + P_b - P_0|/P_0 < 10^{-8}$; see Eq. (34). This verifies, at least partially, the correctness of the theory and its numerical implementation.

Moving on to the analysis of the propelling force F_x, we clearly see that the peaks of the force correlate with the dips of the transmitted surface wave. Unlike the case of a plane wave, see Figs. 2 and 3, where small peaks are superimposed on a significant background, the force dependence now is a set of easily recognizable narrow peaks with practically no background at $kR \gtrsim 20$. The remarkable feature of F_x is its very large value. Indeed, cF_x/P_0 can exceed 1.4. For an ideal absorber in vacuum illuminated by a plane wave, the corresponding ratio for a unit area would be 1.

Regarding the transverse force F_y, its behavior at small kR shows an attraction $F_y < 0$ which increases with kR. However, at larger kR the force starts to exhibit strong repulsive peaks that also correlate with the position of WGM resonances. The magnitude of this force exceeds significantly the propulsion force F_x.

To understand the role of the waveguiding surface, we also investigated the case in which the interaction with the surface is neglected. This is a common approximation since in this case the resonator is excited by an evanescent tail but it is assumed to be surrounded by an infinitely extended uniform medium (with

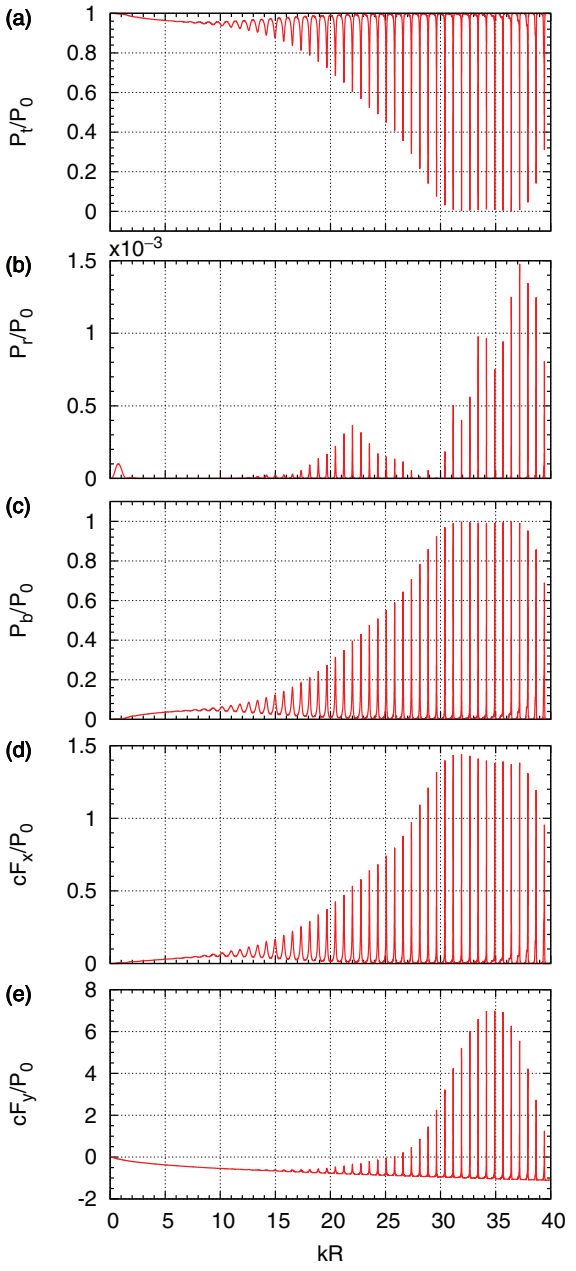

FIG. 4. (Color online) Power of the (a) transmitted and (b) reflected surface waves, and (c) power of the bulk waves, (d) propulsion force, and (e) transverse force as functions of kR for $n_s = 1.4$ and $kd = 1.5$.

$\varepsilon_b = 1$ in our case). Such a case can be directly obtained from our results if we set $r_{bp} = 0$ in Eq. (23). However, we kept r_{bp} in Eq. (32) to model the reflection of the excited bulk waves. The results of scattering in this approximation are shown in Fig. 5. Neglecting the interaction with the surface breaks down the self-consistency of the solution. As a result, the power balance is also violated. This is especially pronounced in the most interesting regime of large $kR > 10$. This can be attributed to the unlimited power that can be provided by the infinitely extended evanescent tail. The neglect of the interaction also overestimates the propulsion force. For the transverse force, it

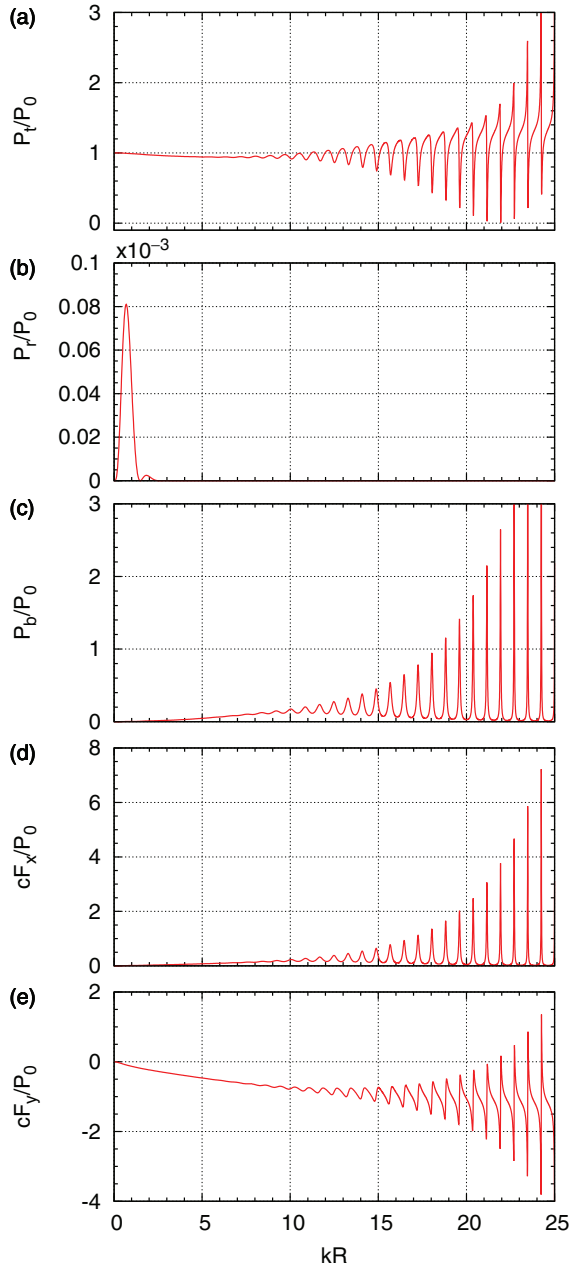

FIG. 5. (Color online) Same as Fig. 4 but assuming that there is no reflection from the surface at $y = -R - d$.

not only gives the incorrect magnitude for the force but it also changes the symmetry of the peaks.

To explain the origin of the large force $cF_x/P_0 > 1$ in Fig. 4, we study the balance of the electromagnetic momentum flow. By using (4) with $\varepsilon_p = -2$ and $\varepsilon_b = 1$, we obtain the phase velocity for the initial surface wave $v_{\rm ph} = \omega/h_0 = c/\sqrt{2}$ and, therefore, $M_0 = P_0\sqrt{2}/c$. Assuming a complete absorption of the transferred momentum gives the maximum value of force $F_x/M_0 \approx 1$. This agrees with the maximum values of force in Fig. 4. Thus, our results suggest that the maximum force that we observe is very close to the value of the momentum flow of the initial surface wave (see Fig. 4). The maximum value of force is reached when the transmitted

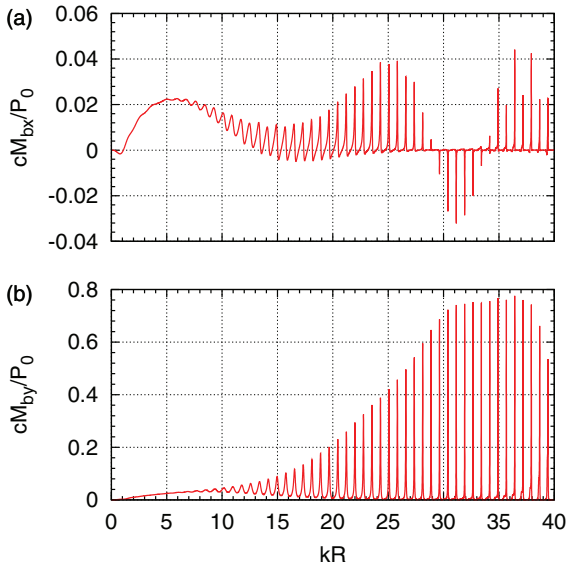

FIG. 6. (Color online) Momentum flow of the bulk radiation in the x and y directions as functions of kR.

surface waves are almost completely suppressed and the initial power goes into bulk waves via the excitation of WGMs.

We can also look more closely at the momentum balance not only when the force reaches maxima but also for arbitrary values of kR. Figure 6 shows the dependence of cM_{bx}/P_0 and cM_{by}/P_0 defined by Eq. (36) on kR. We see that the momentum cM_{bx}/P_0 carried by the bulk waves in the x direction is rather small.

The numerical difference between ΔM calculated using (37) and F_x calculated using (28) and (29) remains $c|\Delta M - F_x|/P_0 < 10^{-8}$ for $0 < kR < 40$. Thus, the force on the cylinder coincides with ΔM, as required by (37). We can conclude that the propelling force on the cylinder can be found either by calculating the force directly (using the Lorentz formula or the Maxwell tensor) or by calculating the change in the momentum flow. This means that there is no lateral force on the metal half-space. However, in some cases the lateral force may appear as a result of beam transmission into a dielectric medium [35]. The verification of the momentum balance also confirms that (35) is the correct expression for the momentum flow of the surface wave. In the regime when the excitation of WGMs is important, the contribution of the momentum flow of the bulk waves is rather small (although their power is large) and the force can be estimated using the following approximate formula:

$$F_x \approx \frac{n_{\rm ph}P_0}{c}\left(1 - \frac{P_t}{P_0}\right) \approx \frac{n_{\rm ph}P_0}{c}\frac{P_b}{P_0}. \qquad (39)$$

Increasing the force F_x (for a fixed P_0) can in principle be achieved either by decreasing P_t or increasing $n_{\rm ph}$. However, these two methods affect each other. For example, increasing $n_{\rm ph}$ causes a phase mismatch between the initial surface wave and WGMs, low excitation for WGMs, and therefore a higher value of P_t.

The bulk radiation has a significant momentum flow in the $+y$ direction. Interestingly, its dependence on kR is similar to that for the propelling force F_x but it is smaller by

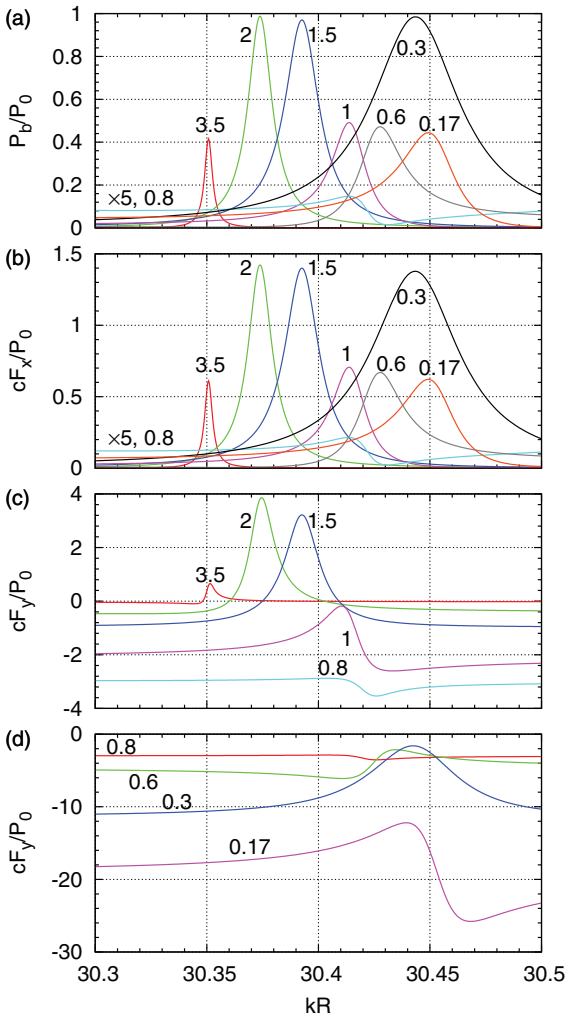

FIG. 7. (Color online) (a) Power of the bulk waves, (b) propulsion force, and (c) and (d) transverse force as functions of kR for various values of kd (labeled next to the corresponding curves). The curves on frames (a) and (b) with the label ×5 are multiplied by a factor of 5 to increase their visibility.

approximately a factor of 2. The existence of this momentum as well as the transverse force on the cylinder results in a corresponding force on the metal half-space.

After investigating the behavior of powers and forces in a wide range of kR, we now focus on a single resonance and investigate its behavior for various cylinder-to-surface distances. The results are summarized in Fig. 7. We start by looking at the power of the bulk waves shown in Fig. 7(a). Starting from a large kd, we see that the peak shows a tendency to become wider as kd decreases. The widening of the peak can be explained by the reduction of the Q factor of the WGM due to the interaction with the surface. However, its height exhibits strongly nonmonotonic behavior with two well-defined maxima, at $kd \sim 2$ and $kd \sim 0.3$. Interestingly, the scattering practically vanishes between these points at $kd = 0.8$.

The behavior of the propelling force in Fig. 7(b) correlates well with the behavior of the scattered bulk radiation. The behavior of the transverse force is more complicated. For relatively large distances $kd \gtrsim 1.5$, the force represents a

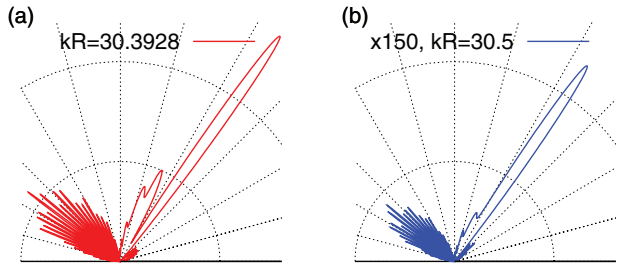

FIG. 8. (Color online) Angular distribution of the power of bulk radiation (a) on-resonance ($kR = 30.3928$) and (b) off-resonance ($kR = 30.5$) for $kd = 1.5$. The grid size is the same on both frames and the off-resonance curve was multiplied by a factor of 150 as indicated.

repulsive peak on top of some attractive background. As the distance becomes smaller, the repulsive peak undergoes significant transformation: its magnitude and shape change. At $kd = 0.8$, it practically vanishes. However, the background shows a clear tendency to become more and more attractive as kd decreases.

Another interesting feature of the force dependence on distance is a shift of the peak that significantly exceeds its width. The shift to higher kR values with decreasing kd means that for the same R, the WGM frequency increases. In general, the interaction of a resonator with a waveguide can increase or decrease the resonant frequency [36]. Such shifts are used in sensor applications of resonators [37]. This shift also affects the possibility of experimental observations of the optical propulsion [20,21]. The experiments involve an optical attraction to the surface compensated at short distances by electrostatic repulsion. The steady-state gaps between the particle and the fiber are rather small such that $kd < 1$. It can be concluded from Fig. 7 that there are particles ($kR \gtrsim 30.4$) that can experience a large propelling force at small particle-to-surface separations and an attractive force regardless of the separation. This explains why resonant particles can be radially trapped in the propulsion experiments.

Figure 8 shows the angular distribution of the power of bulk radiation at $kd = 1.5$ for the same peak as investigated in Fig. 7. We clearly see a highly anisotropic scattering both on- and off-resonance. Scattering occurs both in the forward and backward directions. The presence of such anisotropy also explains the smallness of momentum transferred by the bulk waves in the $+x$ direction [see Fig. 6(a)] and its neglect in the approximate formula for the force (39). In general, the oscillations of the radiation pattern appear as the result of the interference in the far-field region of the waves that are emitted directly from the resonator and that are reflected from the metal boundary. Indeed, by looking at the emission of a particular component of the effective current with a fixed n (32) (the case relevant for resonant excitation), we obtain that the far-field pattern behaves as

$$|f(\varphi)|^2 \sim \cos^2[\varphi_r(k_b \cos\varphi)/2 - n\varphi + k_b a \sin\varphi], \qquad (40)$$

where $\varphi_r(h)$ is the phase of the reflection coefficient. Several features are explained by Eq. (40). First, since $\varphi_r(\pm k_b) = \pi$ there is no scattering in the directions $\varphi = 0,\pi$. Second, since n and $k_b a$ are large and of comparable values, the difference

$-n\varphi + k_b a \sin(\varphi)$ changes slowly at small angles and fast at large angles. This explains the slow oscillations of the pattern with φ at $0 < \varphi < \pi/2$ and the fast oscillations at $\pi/2 < \varphi < \pi$. However, one also has to keep in mind that all current components with various azimuthal numbers n emit coherently, and that creates the complex pattern observed in Fig. 8.

V. CONCLUSION

We investigated the force experienced by a microparticle supporting high-Q whispering gallery modes excited by a surface wave. Our approach uses an analytical formulation of the scattering problem based on the representation of the fields outside of the microparticle as excited by effective surface currents with corresponding Green's function. The current distribution and the resultant fields are then calculated numerically by solving a linear system of equations. The force is calculated by substituting the fields into either the Lorentz formula or the Maxwell tensor.

We showed that the excitation of WGMs by an incident surface wave results in suppression of the transmitted surface wave and enhancement of scattering into bulk waves. The bulk radiation has a strongly anisotropic angular distribution that highlights the importance of including the interaction between the microparticle and the guiding surface. The efficiency of the resonant excitation depends nonmonotonically on the resonator-to-surface distance. Interestingly, there can be a particular distance where the resonant excitation is strongly suppressed. On the other hand, the width of the scattering peak increases monotonically as the microparticle comes closer to the surface.

We showed that the resonant peaks of the propelling force F_x on the microparticle correlate with the suppression of the transmitted surface wave and enhancement of the scattered bulk radiation. Our results for the force and momentum flow balance are consistent with the momentum flow of the surface wave defined as $M_0 = P_0/v_{\mathrm{ph}}$, where P_0 is the power and v_{ph} is the phase velocity of the surface wave. The maximum value of force can reach a value that corresponds approximately to a complete transformation of the momentum flow of the incident surface wave. Moreover, our results establish that the slowness of the initial surface wave of power P_0 allows one to achieve $cF_x/P_0 > 1$ even though there is no reflected surface wave and scattered bulk waves transfer very small momentum in the x direction. This means that, in general, the surface waves with smaller phase velocities can create a higher force on microparticles when compared to bulk beams with the same power.

We also show that the transverse force consists of two parts: an attractive nonresonant background and a resonant part. The nonresonant background grows with the decreasing particle-to-surface distance. The shape of the resonant part depends strongly on the parameters: it can show an asymmetric structure as well as strong repulsion. The magnitude of the transverse force can exceed significantly that of the propulsion force.

ACKNOWLEDGMENTS

The work at the University of Nizhny Novgorod was supported in part by the Ministry of Education and Science of the Russian Federation through Agreement No. 14.B37.21.0892. The work at the University of North Carolina at Charlotte was supported by the US Army Research Office (ARO) under Contract No. W911NF-09-1-0450 (J. T. Prater) and from the National Science Foundation (NSF) under Grant No. ECCS-0824067.

[1] A. Ashkin, Proc. Natl. Acad. Sci. (USA) **94**, 4853 (1997).
[2] A. Ashkin and J. M. Dziedzic, Phys. Rev. Lett. **38**, 1351 (1977).
[3] P. Chýlek, J. T. Kiehl, and M. K. W. Ko, Phys. Rev. A **18**, 2229 (1978).
[4] A. N. Oraevsky, Quantum Electron. **32**, 377 (2002).
[5] V. Ilchenko and A. Matsko, IEEE J. Sel. Top. Quantum Electron. **12**, 15 (2006).
[6] V. N. Astratov, in *Photonic Microresonator Research and Applications*, Springer Series in Optical Sciences Vol. 156, edited by I. Chremmos, O. Schwelb, and N. Uzunoglu (Springer, New York, 2010), Chap. 17, pp. 423–457.
[7] W. N. Irvine, J. Opt. Soc. Am. **55**, 16 (1965).
[8] H. Jaising and O. Helleso, Opt. Commun. **246**, 373 (2005).
[9] J. Ng and C. T. Chan, Appl. Phys. Lett. **92**, 251109 (2008).
[10] J. J. Xiao, J. Ng, Z. F. Lin, and C. T. Chan, Appl. Phys. Lett. **94**, 011102 (2009).
[11] L. Xu, Y. Li, and B. Li, New J. Phys. **14**, 033020 (2012).
[12] H. Jaising, K. Grujic, and O. Helleso, Opt. Rev. **12**, 4 (2005).
[13] B. S. Schmidt, A. H. J. Yang, D. Erickson, and M. Lipson, Opt. Express **15**, 14322 (2007).
[14] M. Povinelli, M. Loncar, M. Ibanescu, E. Smythe, S. Johnson, F. Capasso, and J. Joannopoulos, Opt. Lett **30**, 3042 (2005).
[15] M. Li, W. H. P. Pernice, and H. X. Tang, Nat. Photon. **3**, 464 (2009).
[16] M. Eichenfield, C. P. Michael, R. Perahia, and O. Painter, Nat. Photon. **1**, 416 (2007).
[17] M. Barth and O. Benson, Appl. Phys. Lett. **89**, 253114 (2006).
[18] J. Ma, L. J. Martinez, and M. L. Povinelli, Opt. Express **20**, 6816 (2012).
[19] J. Hu, S. Lin, L. C. Kimerling, and K. Crozier, Phys. Rev. A **82**, 053819 (2010).
[20] Y. Li, O. V. Svitelskiy, A. V. Maslov, D. Carnegie, E. Rafailov, and V. N. Astratov, in *IEEE Proceedings of the 14th International Conference on Transparent Optical Networks (ICTON-2012)* (IEEE, Piscataway, NJ, 2012), paper no. Tu.A6.2.
[21] Y. Li, O. V. Svitelskiy, A. V. Maslov, D. Carnegie, E. Rafailov, and V. N. Astratov, Light: Sci. Appl. **2**, e64 (2013).
[22] O. Svitelskiy, Y. Li, A. Darafsheh, M. Sumetsky, D. Carnegie, E. Rafailov, and V. N. Astratov, Opt. Lett. **36**, 2862 (2011).
[23] R. N. C. Pfeifer, T. A. Nieminen, N. R. Heckenberg, and H. Rubinsztein-Dunlop, Rev. Mod. Phys. **79**, 1197 (2007).
[24] A. V. Boriskin, S. V. Boriskina, A. Rolland, R. Sauleau, and A. I. Nosich, J. Opt. Soc. Am. A **25**, 1169 (2008).
[25] Z. Guo and H. Quan, J. Heat Transf.: Trans. ASME **129**, 44 (2007).
[26] V. I. Kalinichev and P. N. Vadov, Radiotekhnika i Elektronika **33**, 464 (1988).

[27] I. D. Chremmos and N. K. Uzunoglu, J. Opt. Soc. Am. A **21**, 839 (2004).
[28] A. G. Yarovoy, Microwave Opt. Technol. Lett. **7**, 178 (1994).
[29] S. V. Boriskina and A. I. Nosich, Microwave Opt. Technol. Lett. **13**, 169 (1996).
[30] R. F. Harrington, J. Electromagn. Waves Appl. **3**, 1 (1989).
[31] D. Colton and R. Kress, *Integral Equation Method in Scattering Theory* (Wiley, New York, 1983).
[32] A. V. Maslov, M. I. Bakunov, and C. Z. Ning, J. Appl. Phys. **99**, 024314 (2006).
[33] J. Brown, Proc. IEE **113**, 27 (1966).
[34] H. A. Haus and H. Kogelnik, J. Opt. Soc. Am. **66**, 320 (1976).
[35] M. Mansuripur, Opt. Express **12**, 5375 (2004).
[36] Z. Guo, H. Quan, and S. Pau, J. Phys. D.: Appl. Phys. **39**, 5133 (2006).
[37] K. R. Hiremath and V. N. Astratov, Opt. Express **16**, 5421 (2008).